Electronic Supplementary Material (ESI) for Lab on a Chip.


# Supplementary Material to:

# On the compatibility of single-cell microcarriers (nanovials) with microfluidic impedance cytometry

Cristian Brandi,[a,§] Adele De Ninno,[b,§] Filippo Ruggiero,[b] Emanuele Limiti,[c] Franca Abbruzzese,[c] Marcella Trombetta,[d] Alberto Rainer,[c,e] Paolo Bisegna,[a] and Federica Caselli [a,*]

[a] *Department of Civil Engineering and Computer Science, University of Rome Tor Vergata, Rome, Italy. E-mail: caselli@ing.uniroma2.it*

[b] *Italian National Research Council - Institute for Photonics and Nanotechnologies (CNR - IFN), Rome, Italy.*

[c] *Department of Engineering, Università Campus Bio-Medico di Roma, via Álvaro del Portillo, 21, 00128, Rome, Italy.*

[d] *Department of Science and Technology for Sustainable Development and One Health, Università Campus Bio-Medico di Roma, via Álvaro del Portillo 21, 00128, Rome, Italy.*

[e] *National Research Council - Institute of Nanotechnology (CNR-NANOTEC), c/o Campus Ecotekne, 73100 Lecce, Italy.*

*(§, equal contribution)*

## Section S1: Bipolar Gaussian templateig

Bipolar Gaussian template (Fig. S1) used to fit the event signals:

$$s_f(t) = a_f\left(e^{-\frac{(t-(t_c-\delta/2))^2}{2\sigma^2}} - e^{-\frac{(t-(t_c+\delta/2))^2}{2\sigma^2}}\right) \qquad (2)$$

The template is characterized by the complex frequency-dependent amplitude $a_f$, the peak-width control $\sigma$, the peak-to-peak time $\delta$ and the central time $t_c$. The complex amplitude $a_f$ is converted in modulus and phase. One low frequency is used in the present work ($f = 0.5$ MHz). Since at low frequencies signal amplitude is proportional to cell volume, its cube root represents an electrical measure of the cell diameter (the electrical diameter).

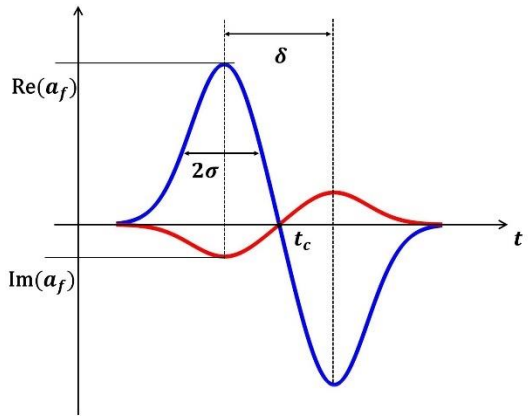


**Fig. S1** Bipolar Gaussian template.

## Section S2: Finite element model of the microfluidic impedance cytometer

The model of the electric current conduction in a microfluidic impedance cytometer developed in Ref.[1] is extended here to account for the presence of the nanovial. The cytometer is modeled as the union of three homogeneous conducting regions $\Omega_n$, $\Omega_c$ and $\Omega_b$, representing the nanovial domain, the cell cytoplasm, and the buffer fluid, respectively. Their complex conductivities $\sigma_n^*$, $\sigma_c^*$ and $\sigma_b^*$ are given by $\sigma_k^* = \sigma_k + i\omega\varepsilon_k\varepsilon_v$, where $\varepsilon_v$ is the vacuum permittivity and $\sigma_k$ and $\varepsilon_k$ are the conductivity and relative permittivity of the media, respectively; moreover, $i$ is the imaginary unit, and $\omega$ denotes the circular frequency. The cell membrane is treated as a 2-D interface $\Gamma$ with conductance $G_{mem}$ and capacitance $C_{mem}$ per unit area, respectively, given by the electric conductivity $\sigma_m$ and permittivity $\varepsilon_m\varepsilon_v$ of the lipid bilayer, divided by its thickness. Therefore, the interface admittance per unit area is $Y = G_{mem} + i\omega C_{mem}$. It turns out that $Y \approx i\omega C_{mem}$, since $G_{mem} \ll \omega C_{mem}$ in the radio-frequency range, and hence, the cell membrane essentially behaves as a capacitor. The finite interface admittance causes the electric potential to jump across the cell membrane.

In the Fourier domain, the problem of determining the electric potential $v$ in the cytometer is stated as follows:

$$-div(\sigma^*\nabla v) = 0, \qquad \text{in } \Omega_n \cup \Omega_c \cup \Omega_b \qquad (1)$$

$$[\![\sigma^*\nabla v \cdot n]\!] = 0, \qquad \text{on } \Gamma \qquad (2)$$

$$Y[\![v]\!] = \sigma^*\nabla v \cdot n, \qquad \text{on } \Gamma \qquad (3)$$

along with potential and flux continuity at the nanovial-buffer interface. Here $div$ and $\nabla$ are the divergence and gradient operators, respectively, a dot denotes the scalar product, $n$ is the normal unit vector to $\Gamma$ pointing outside $\Omega_c$, $[\![\cdot]\!]$ brackets denote the jump of the enclosed quantity across the membrane, and finally, $\sigma^* = \sigma_n^*$ in $\Omega_n$, $\sigma^* = \sigma_c^*$ in $\Omega_c$, and $\sigma^* = \sigma_b^*$ in $\Omega_b$. Equation (1) governs the electric conduction in the nanovial domain, in the cell cytoplasm, and in the fluid, equation (2) accounts for the continuity of the current flux density through the cell membrane, and equation (3) describes the membrane electric behavior.

An insulating boundary condition is applied on the cytometer surface not covered by electrodes ($\partial\Omega_{ne}$)

$$\sigma^*\nabla v \cdot n = 0, \qquad \text{on } \partial\Omega_{ne} \qquad (4)$$

where $n$ is the outward normal unit vector. On the $i$-th electrode ($\partial\Omega_{e_i}$), the following electrode equation holds:

$$Y_e(V_i - v) = \sigma^*\nabla v \cdot n, \qquad \text{on } \partial\Omega_{e_i} \qquad (5)$$

where $Y_e = G_e + i\omega C_e$ is the electrode admittance per unit area, expressed in terms of the electrode conductance $G_e$ and capacitance $C_e$ per unit area, $V_i$ is the electrode potential, and the right-hand side is the current density through the electrode. In the radio-frequency range $G_e$ is usually negligible with respect to $\omega C_e$.

Problem (1)-(5) is recast into the following weak formulation:

$$\int_{\Omega_n\cup\Omega_c\cup\Omega_b} \sigma^*\nabla v \cdot \nabla w \, dx + \int_\Gamma Y[\![v]\!][\![w]\!] \, ds + \sum_i \int_{\partial\Omega_{e_i}} Y_e v w \, ds = \sum_i \int_{\partial\Omega_{e_i}} Y_e V_i w \, ds$$

where $w$ is an arbitrary test function and $dx$ and $ds$ denote volume and surface integration, respectively. Exploiting this formulation, the potential distribution $v$ induced by prescribed electrode potentials $V_i$ can be uniquely determined. The resulting electric current $I_i$ through the $i$-th electrode can then be computed as

$$I_i = \int_{\partial\Omega_{e_i}} \sigma^*\nabla v \cdot n \, ds = \int_{\partial\Omega_{e_i}} Y_e(V_i - v) \, ds \, .$$

The model is implemented in COMSOL Multiphysics using the *Weak form* physics. The device geometric model is shown in Fig. S2. Material parameters and device geometric parameters are listed in Tables S1 and S2 respectively.

Details of the cell-loaded nanovial geometry are given in Section S3 and Table S3. Unless otherwise specified in the text, the nanovial is assumed centered in the channel cross section, with its cavity oriented towards $-y$.

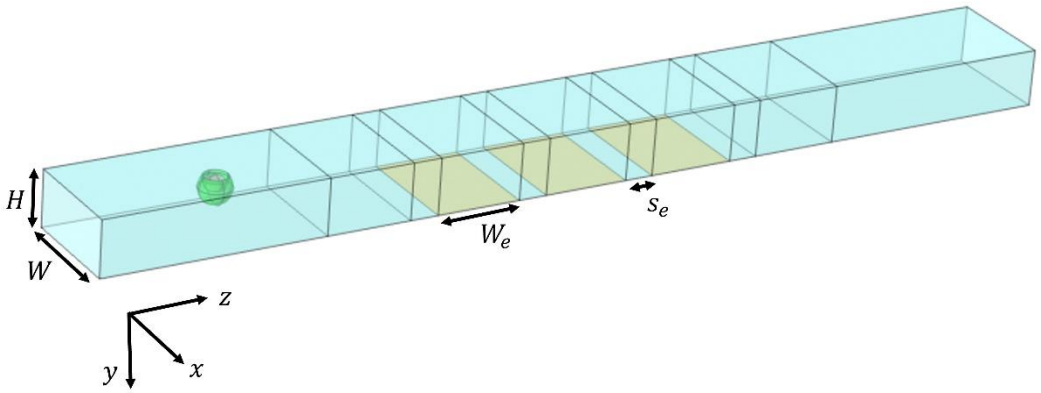


**Fig. S2** Geometric model of the microfluidic impedance cytometer.

**Table S1** Material parameters used in the numerical simulations (unless otherwise specified).

| $C_e$ | $\sigma_b$ | $\varepsilon_b$ | $\sigma_n$ | $\varepsilon_n$ | Cell type | $\sigma_c$ | $\varepsilon_c$ | $G_{mem}$ | $C_{mem}$ |
|---|---|---|---|---|---|---|---|---|---|
| 0.144 F/m$^2$ | 0.9 S/m | 80 | 0.6 S/m | 80 | reference | 0.5 S/m | 60 | 0 S/m$^2$ | 0.01 F/m$^2$ |
| | | | | | increased $G_{mem}$ | 0.7 S/m | 70 | $10^6$ S/m$^2$ | 0.01 F/m$^2$ |
| | | | | | reduced $C_{mem}$ | 0.5 S/m | 60 | 0 S/m$^2$ | 0.005 F/m$^2$ |

**Table S2** Geometric parameters of the simulated microfluidic impedance cytometer (cf Fig. S2).

| $W$ | $H$ | $W_e$ | $s_e$ |
|---|---|---|---|
| 120 µm | 60 µm | 90 µm | 30 µm |

## Section S3: Geometric model of the cell-loaded nanovial

The geometric model of the cell-loaded nanovial comprises two entities: the nanovial and the cell adherent to its cavity. A 3D axisymmetric model is built, by defining the nanovial and cell profiles in a $x_w y_w$ workplane (Fig. S3). Following Liu et al.,[2] the nanovial geometry is defined by the difference of two circles with centers $\boldsymbol{C_1}$ and $\boldsymbol{C_2}$ and radii $R_1$ and $R_2$ respectively. An original parametric model is developed to define the cell profile. A cubic Bezier curve is used, defined by control points $\boldsymbol{P_1}$ to $\boldsymbol{P_4}$ and associated unitary weights. The points $\boldsymbol{P_1}$ and $\boldsymbol{P_4}$ (which are interpolation points) are given by:

$$\boldsymbol{P_1} = \boldsymbol{C_2} + R_2 \cdot \hat{\boldsymbol{e}} \quad (2)$$

$$\boldsymbol{P_4} = \boldsymbol{C_2} + (H_{\text{cell}} - R_2) \cdot \hat{\boldsymbol{j}} \quad (3)$$

where $\hat{\boldsymbol{e}} = (sin\,\alpha\,, -cos\,\alpha)$, with $\alpha = sin^{-1}((aD_{\text{cell}}/2)/R_2)$, and $\hat{j}$ is the unitary vector of the $y_w$ axis. The parameters $H_{\text{cell}}$ and $aD_{\text{cell}}$ respectively modulate the cell height and the cell adhesion diameter. The points $\boldsymbol{P_2}$ and $\boldsymbol{P_3}$ (through which the tangent at the Bezier curve in $\boldsymbol{P_1}$ and $\boldsymbol{P_4}$ respectively passes) are given by:

$$\boldsymbol{P_2} = \boldsymbol{P_1} + (R_2/2) \cdot \hat{\boldsymbol{t}} \quad (4)$$

$$\boldsymbol{P_3} = \boldsymbol{P_4} + (R_2/2) \cdot \hat{\boldsymbol{t}} \quad (5)$$

where $\hat{\boldsymbol{t}} = (cos\,\alpha\,, sin\,\alpha)$ and $\hat{t}$ is the unitary vector of the $x_w$ axis. The parameter values used in the numerical simulations are indicated in Table S3.

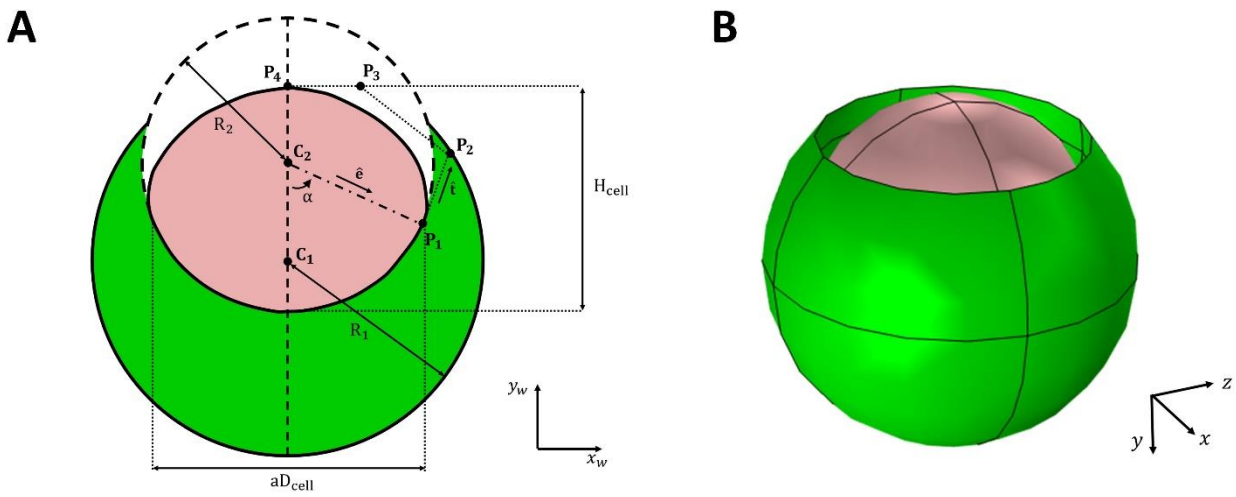


**Fig. S3** (A) Geometric model of the cell-loaded nanovial in the $x_w y_w$ workplane. (B) 3D geometric model obtained via revolution around $y_w$.

**Table S3** Geometric parameter values of the cell-loaded nanovial.

| $\boldsymbol{C_1}$ | $R_1$ | $\boldsymbol{C_2}$ | $R_2$ | $H_{\text{cell}}$ | $aD_{\text{cell}}$ |
|---|---|---|---|---|---|
| $[0, 0]$ | 17.5 µm | $[0, 0.5R_1]$ | $0.75R_1$ | 20 µm | 24 µm |

## Section S4: Calibration of simulation data

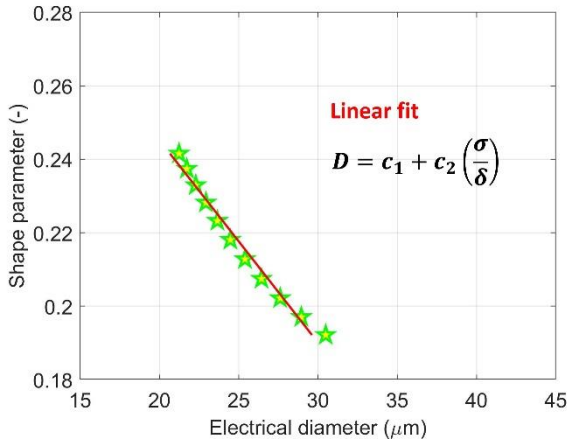


**Fig. S4** Linear fit of the relationship between the electrical diameter $D$ and the shape parameter $\sigma/\delta$ based on simulation data. The relevant parameters are $c_1 = 64$ µm and $c_2 = -181$ µm, which are in reasonable agreement with those obtained for the experimental data ($c_1 = 63$ µm and $c_2 = -161$ µm, see section 3.2 of the main text). Implementing the calibration on experimental data rather than on simulation data allows to automatically handle minor variations of the experimental setup (e.g., chip to chip variability, buffer conductivity)[3].

## Section S5: In-silico analysis of orientation blurring

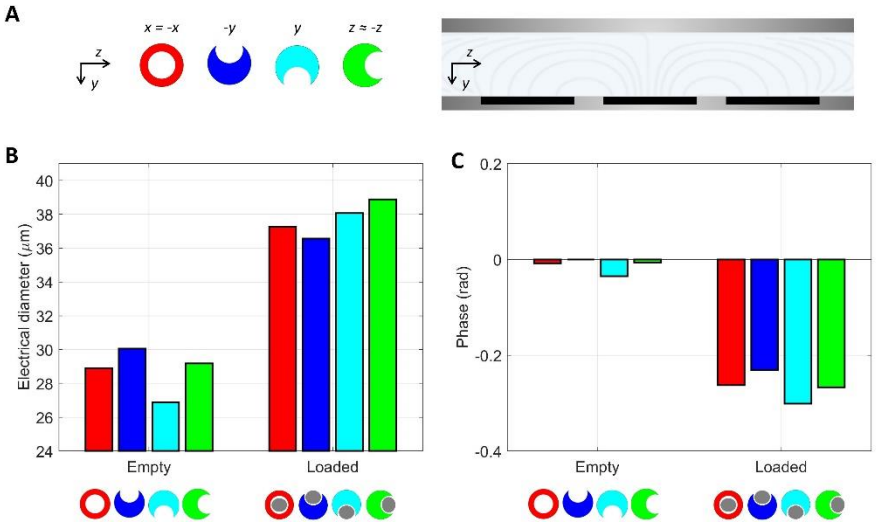


**Fig. S5** (A) Schematic representation of empty nanovials with their revolution axis along $x, -y, y, z$ (the sensing zone is also illustrated as reference). From the point of view of the generated impedance signals, the orientations along $-x$ and $-z$ are equivalent to those along $x$ and $z$, respectively. (B) Electrical diameter and electrical phase of empty/loaded nanovials passing through the sensing zone with different orientations. Orientation blurring can be quantified as follows (mean ± std): empty-nanovial diameter = 28.85 ± 1.05 µm; loaded-nanovial diameter = 37.82 ± 0.95 µm; empty-nanovial phase = -0.01 ± 0.01 rad; loaded-nanovial phase = -0.26 ± 0.02 rad. Accordingly, orientation blurring may be neglected in most situations.

## Section S6: Examples of misclassification

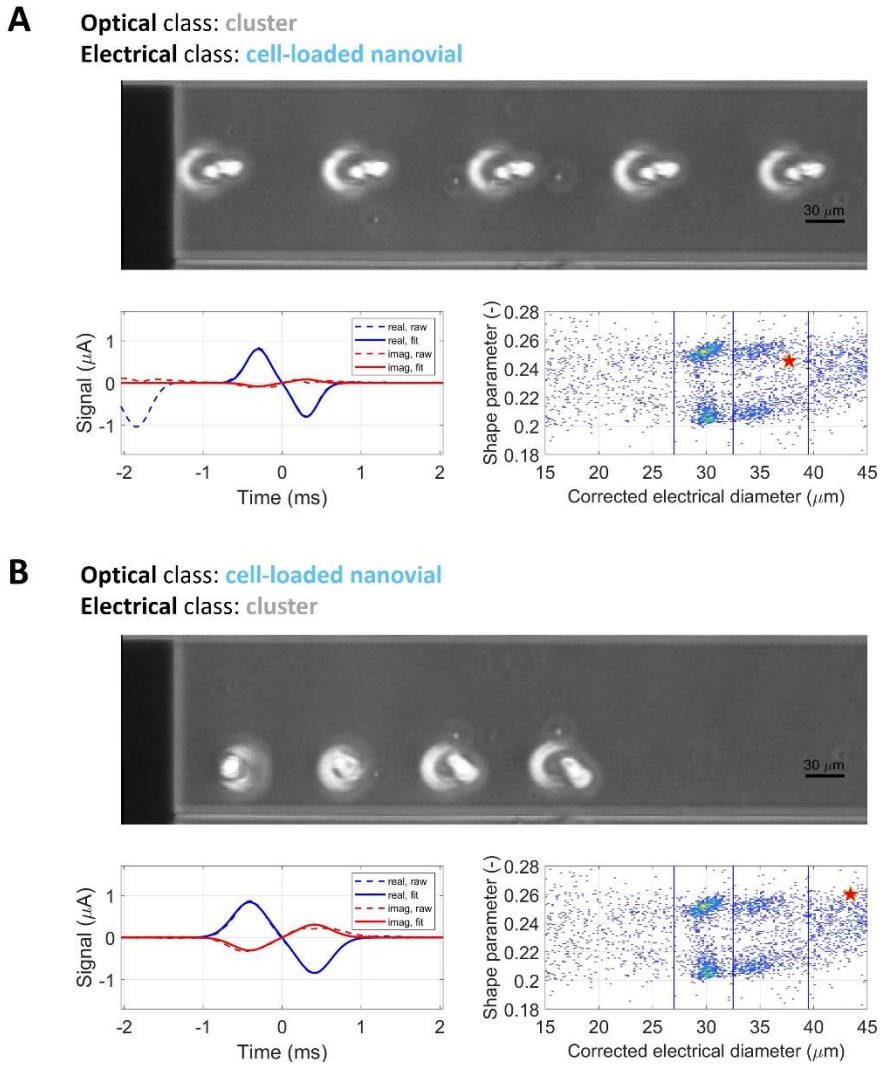


**Fig. S6** Overlay of consecutive snapshots, electrical signals, and data point localization in the density plot of the shape parameter against the corrected electrical diameter for: (A) a cluster composed of one nanovial and two cells that is misclassified as a cell-loaded nanovial based on the corrected electrical diameter, (B) A cell-loaded nanovial that is misclassified as a cluster based on the corrected electrical diameter. It can be noticed that the large cell partially comes out of the nanovial cavity.

## Section S7: Impedance variations induced by Triton-X exposure

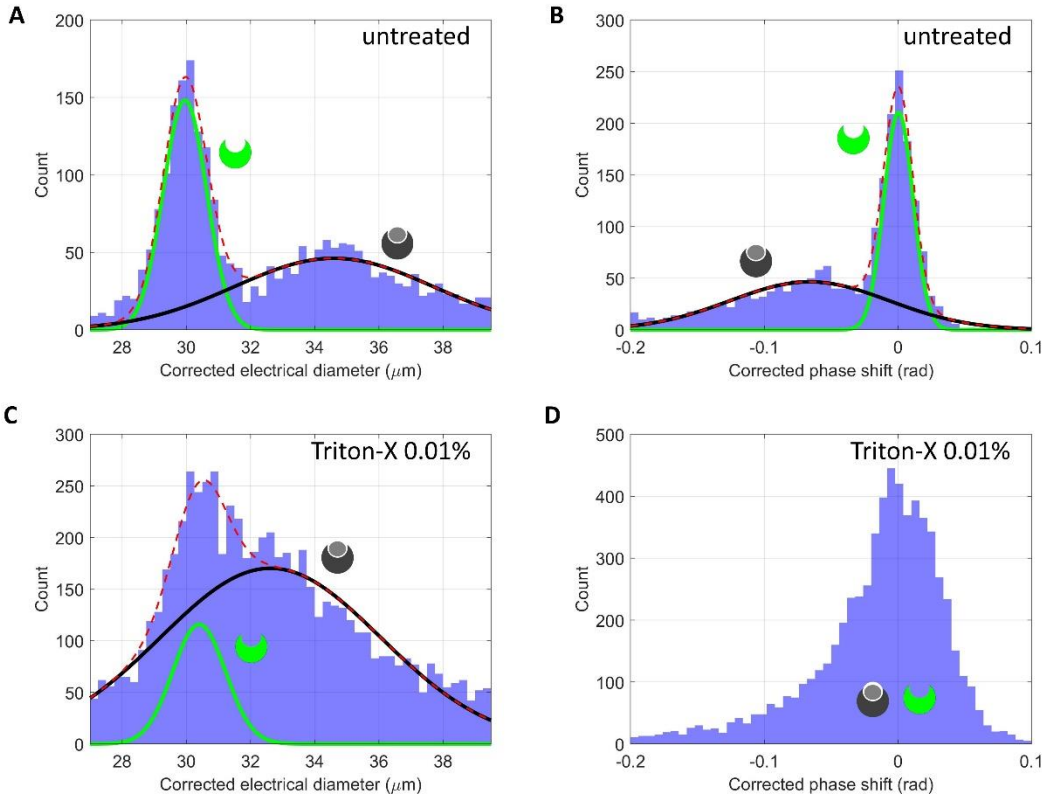


**Fig. S7** Histograms of the electrical features (0.5 MHz) relevant to (A, B) a control sample and (C, D) a sample exposed to Triton-X at 0.01% after cell-nanovial incubation. The corrected electrical diameter is shown in panels (A, C). In both cases (untreated/treated), the histogram is described by the sum (red, dashed) of two Gaussian distributions (green, empty nanovials; black, loaded nanovials, as verified by optical inspection). The mean electrical diameter of the empty nanovial population is about 30 µm, for both samples, while the mean electrical diameter of the loaded population is 34.5 µm for the control sample and 32.6 µm for the treated sample. The reduction of electrical diameter after Triton-X exposure (which induces cell membrane permeabilization) agrees with the numerical analysis reported in Section 4.3 and Fig. 8(A) of the main text. The corrected phase shift is shown in panels (B, D). It is obtained from the phase shift with respect to empty nanovials by applying a compensation procedure for position blurring analogous to that used for the electrical diameter. Specifically: Corrected phase shift = phase shift $-\left(c_1 + c_2(\sigma/\delta)\right)$, where $c_1$ and $c_2$ are calibration coefficients obtained via linear fitting in the shape-parameter vs phase-shift plane. For the untreated sample (panel B), two Gaussian distributions can be recognized: the loaded population (black) exhibits a phase shift of -0.07 rad with respect to the empty population. On the other hand, for the treated sample the phase of the loaded nanovials is similar to that of the empty nanovials (the two distributions overlap and cannot be individually fitted from the histogram). These results are in qualitative agreement with the numerical analysis reported in Fig. 8(B) of the main text.

## References


1 F. Caselli, P. Bisegna and F. Maceri, *Journal of Microelectromechanical Systems*, 2010, **19**, 1029–1040.

2 Q. Liu, M. Zhao, S. Mytnyk, B. Klemm, K. Zhang, Y. Wang, D. Yan, E. Mendes and J. H. van Esch, *Angewandte Chemie*, 2019, **131**, 557–561.

3 F. Caselli and P. Bisegna, *Med Eng Phys*, 2017, **48**, 81–89.